J|A|C|S ARTICLES

Published on Web 03/15/2010

Dynamic Active-Site Protection by the *M. tuberculosis* Protein Tyrosine Phosphatase PtpB Lid Domain

E. Megan Flynn,[†] Jeffrey A. Hanson,[‡,§] Tom Alber,*[,†] and Haw Yang*[,‡,§]

Department of Molecular and Biology and QB3 Institute and Department of Chemistry, University of California, Berkeley, California 94720, and Department of Chemistry, Princeton University, Princeton, New Jersey 08544

Received November 25, 2009; E-mail: hawyang@princeton.edu; tom@alber.berkeley.edu

Abstract: The *Mycobacterium tuberculosis* protein tyrosine phosphatase PtpB shows resistance to the oxidative conditions that prevail within an infected host macrophage, but the mechanism of this molecular adaptation is unknown. Crystal structures of PtpB revealed previously that a closed, two-helix lid covers the active site. By measuring single-molecule Förster-type resonance energy transfer to probe the dynamics of two helices that constitute the lid, we obtained direct evidence for large, spontaneous opening transitions of PtpB with the closed form of both helices favored ~3:1. Despite similar populations of conformers, the two helices move asynchronously as demonstrated by different opening and closing rates under our experimental conditions. Assuming that lid closure excludes oxidant, the rates of opening and closing quantitatively accounted for the slow observed rate of oxidative inactivation. Increasing solvent viscosity using glycerol but not PEG8000 resulted in higher rates of oxidative inactivation due to an increase in the population of open conformers. These results establish that the rapid conformational gating of the PtpB lid constitutes a reversible physical blockade that transiently masks the active site and retards oxidative inactivation.

Introduction

Proteins carry out a variety of complicated functions such as catalysis, signaling, and motility. Many of these important activities utilize thermally driven, large-amplitude conformational changes that cannot be readily captured by static crystallographic structures. In contrast to small-molecule reactions for which reactivity can be inferred from molecular structure, a general approach for predicting the roles of conformational changes in protein reactivity and function from static crystallographic structures has yet to come to light. Much recent work has focused on this issue (for reviews, see refs 1−11); however, conventional ensemble experiments, such as NMR and optical spectroscopy, which contribute a great deal of our current understanding of conformational dynamics, are most sensitive to local fluctuations in on very short time scales and generally require additional measurements to define the nature of the conformational changes detected.[5,12−16] A remaining challenge in linking protein conformation and function is to define the physical nature of large-amplitude conformational transitions on biologically relevant millisecond to minute time scales.

To implement a strategy to characterize transient, large-amplitude conformational transitions in proteins, we began by asking the following basic questions: How many conformational states can a protein sample on the functionally important time scale? What are the interconversion rates between states? How do ligand binding or interactions with other proteins modulate the motions? What functional roles do these motions play? It is important to note that only when the range of motion and the conformation−transition kinetics are simultaneously determined can the "dynamics" be properly defined.[17] In this regard, single-molecule Förster-type resonance energy transfer (FRET)

[†] Department of Molecular and Biology and QB3 Institute, University of California.
[‡] Department of Chemistry, University of California.
[§] Department of Chemistry, Princeton University.

(1) Hammes-Schiffer, S.; Benkovic, S. J. *Annu. Rev. Biochem.* **2006**, *75*, 519–541.
(2) Gunasekaran, K.; Ma, B. Y.; Nussinov, R. *Proteins: Struct. Funct. Bioinf.* **2004**, *57*, 433–443.
(3) Callender, R.; Dyer, R. B. *Chem. Rev.* **2006**, *106*, 3031–3042.
(4) Daniel, R. M.; Dunn, R. V.; Finney, J. L.; Smith, J. C. *Annu. Rev. Biophys. Biomol. Struct.* **2003**, *32*, 69–92.
(5) Boehr, D. D.; Dyson, H. J.; Wright, P. E. *Chem. Rev.* **2006**, *106*, 3055–3079.
(6) Hubbell, W. L.; Cafiso, D. S.; Altenbach, C. *Nat. Struct. Biol.* **2000**, *7*, 735–739.
(7) Henzler-Wildman, K.; Kern, D. *Nature* **2007**, *450*, 964–972.
(8) Michalet, X.; Weiss, S.; Jager, M. *Chem. Rev.* **2006**, *106*, 1785–1813.
(9) Boehr, D. D.; Nussinov, R.; Wright, P. E. *Nat. Chem. Biol.* **2009**, *5*, 789–796.
(10) Russel, D.; Lasker, K.; Phillips, J.; Schneidman-Duhovny, D.; Velazquez-Muriel, J. A.; Sali, A. *Curr. Opin. Cell Biol.* **2009**, *21*, 97–108.
(11) Hanson, J.; Tan, Y.-W.; Yang, H. In *Single Particle Tracking and Single-Molecule Energy Transfer: Applications in the Bio and Nano Sciences*; Brauchle, C., Lamb, D., Michaelis, J., Eds.; Wiley-VCH: Weinheim, 2009.
(12) Williams, J. C.; Mcdermott, A. E. *Biochemistry* **1995**, *34*, 8309–8319.
(13) Rozovsky, S.; McDermott, A. E. *J. Mol. Biol.* **2001**, *310*, 259–270.
(14) Eisenmesser, E. Z.; Millet, O.; Labeikovsky, W.; Korzhnev, D. M.; Wolf-Watz, M.; Bosco, D. A.; Skalicky, J. J.; Kay, L. E.; Kern, D. *Nature* **2005**, *438*, 117–121.
(15) Beach, H.; Cole, R.; Gill, M. L.; Loria, J. P. *J. Am. Chem. Soc.* **2005**, *127*, 9167–9176.
(16) McElheny, D.; Schnell, J. R.; Lansing, J. C.; Dyson, H. J.; Wright, P. E. *Proc. Natl. Acad. Sci. U.S.A.* **2005**, *102*, 5032–5037.
(17) Goldstein, H. *Classical Mechanics*; Addison-Wesley: Reading, MA, 1980.

10.1021/ja909968n

experiments, which provide a unique measure of both the time scale and the magnitude of structural fluctuations, have successfully been used to investigate conformational dynamics in biological systems.[1,8,11] Using the single-molecule approach and guided by the framework articulated by the questions listed above, a previous work has reached a mechanistic understanding of the role of conformational dynamics in protein function for proteins such as *E. coli* adenylate kinase.[18] Developing a deeper understanding of large-amplitude conformation transitions in proteins requires an examination of the structural basis of flexibility and its underlying molecular mechanics.

In this context, we report a study of the protein tyrosine phosphatase B (PtpB) from *Mycobacterium tuberculosis*, where evidence is presented for large-scale opening and closing motions of a lid that blocks the enzyme active site in the available crystal structures. It is proposed that the mobile lid element may have evolved as a novel means of protecting the active site against host chemical defenses through conformational gating.

Background

Protein tyrosine phosphatases (PTPs) antagonize protein tyrosine kinases to regulate the cellular balance of tyrosine phosphorylation. The targets of tyrosine phosphorylation in turn control the central cellular processes of growth, proliferation, and differentiation.[19] PTPs catalyze dephosphorylation reactions with a cysteine nucleophile, and the low pK_a of this residue is essential for activity.[20] However, this lowered pK_a also renders the catalytic cysteine susceptible to oxidation and inactivation by reactive oxygen species (ROS). ROS control PTP activity in response to physiological cell stimuli such as growth factors, hormones, and UV radiation.[21−25]

Intracellular pathogens such as *Salmonella*, *Yersinia*, and *Mycobacterium* not only infect macrophages that mount a defensive ROS burst but also secrete PTPs into host cells to disrupt signaling pathways and blunt immune responses.[26] The *M. tuberculosis* (*Mtb*) genome encodes two secreted tyrosine phosphatases, PtpA and PtpB, but no tyrosine kinase.[27] A *ptpB* knockout mutant shows growth defects in interferon-γ (IFN-γ)-stimulated macrophages and after 6 weeks in guinea pigs, suggesting that PtpB is important for long-term mycobacterial survival.[28] Although this points to PtpB as a potential drug target for *Mtb* infection,[29,30] the protein substrates and functions of PtpB in host macrophages remain unknown.

Two crystal structures of the *Mtb* PtpB (Figure 1)[31,32] captured the protein in an enzyme/product complex, with inorganic phosphate at the active site (PtpB/PO_4, Figure 1a), and in complex with the inhibitor (oxalylaminomethylene)thiophene sulfonamide (PtpB/OMTS, Figure 1b). A comparison of PtpB with a dual specificity phosphatase (DSP) from *Arabidopsis thaliana* (Figure 1c,d)[33] reveals that the enzyme contains the core PTP fold common to metazoan homologues. Although several sequence insertions are evident in the structural alignment of PtpB with DSP, the most striking feature is the addition of a two-helix lid comprised of helices α7 and α8, which completely buries the enzyme-active site, sequestering the reactive cysteine from solvent. The PtpB/OMTS inhibitor complex structure revealed a displacement of more than 25 Å in the lid helix α8 compared to its PO_4-bound position (Figure 1e). This large displacement of α8 is mediated by extensive contacts with an inhibitor molecule bound to the active site cleft, while the α7 lid helix is only slightly displaced from its position in the PO_4-bound structure. The PtpB/OMTS structure represents a closed or partially open lid conformation, since the enzyme active site remains buried and there is no clear route for inhibitor to access the active site without further lid movement.[31] This hybrid structure demonstrates that the two lid helixes are flexibly

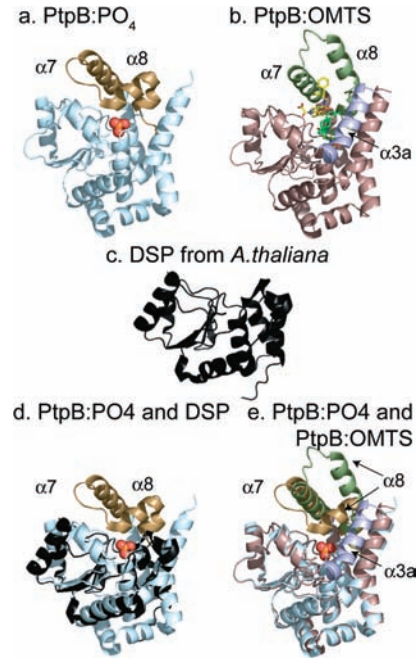

Figure 1. Ribbon diagrams of (a) the PtpB/product complex, PtpB/PO_4 (1YWF[32]), (b) the PtpB/inhibitor complex PtpB:OMTS (2OZ5[31]) and (c) a dual specificity phosphatase (DSP) from *A. thaliana* (1LAR[33]) for comparison. (d) A structural alignment of the PtpB/PO_4 and DSP structures reveals several sequence insertions in PtpB compared with the DSP fold. The most striking of these adaptations is a two-helix lid comprised of helixes α7 and α8, which completely buries the PtpB active site (adjacent to the space filling PO_4 in (a) and (d)). (e) Superposition of the PtpB complexes with PO_4 and OMTS reveals a ∼25 Å displacement of helix α8 and the folding of a new helix (α3a; blue).

(18) Hanson, J. A.; Duderstadt, K.; Watkins, L. P.; Bhattacharyya, S.; Brokaw, J.; Chu, J. W.; Yang, H. *Proc. Natl. Acad. Sci. U.S.A.* **2007**, *104*, 18055–18060.
(19) Alonso, A.; Sasin, J.; Bottini, N.; Friedberg, I.; Friedberg, I.; Osterman, A.; Godzik, A.; Hunter, T.; Dixon, J.; Mustelin, T. *Cell* **2004**, *117*, 699–711.
(20) Zhang, Z. Y.; Dixon, J. E. *Biochemistry* **1993**, *32*, 9340–9345.
(21) Finkel, T. *Curr. Opin. Cell Biol.* **2003**, *15*, 247–254.
(22) Rhee, S.; Bae, Y.; Lee, S.; Kwon, J. *Sci. STKE* **2000**, *2000*, pe1.
(23) den Hertog, J.; Groen, A.; van der Wijk, T. *Arch. Biochem. Biophys.* **2005**, *434*, 11–15.
(24) Salmeen, A.; Barford, D. *Antiodix. Redox Signal.* **2005**, *7*, 560–577.
(25) Tonks, N. K. *Cell* **2005**, *121*, 667–670.
(26) DeVinney, R.; Steele-Mortimer, O.; Finlay, B. B. *Trends Microbiol.* **2000**, *8*, 29–33.
(27) Cole, S. T. *Nature* **1998**, *393*, 537–544.
(28) Singh, R.; Rao, V.; Shakila, H.; Gupta, R.; Khera, A.; Dhar, N.; Singh, A.; Koul, A.; Singh, Y.; Naseema, M.; Narayanan, P. R.; Paramasivan, C. N.; Ramanathan, V. D.; Tyagi, A. K. *Mol. Microbiol.* **2003**, *50*, 751–762.
(29) Soellner, M. B.; Rawls, K. A.; Grundner, C.; Alber, T.; Ellman, J. A. *J. Am. Chem. Soc.* **2007**, *129*, 9613–9615.
(30) Beresford, N. J.; Mulhearn, D.; Szczepankiewicz, B.; Liu, G.; Johnson, M. E.; Fordham-Skelton, A.; Abad-Zapatero, C.; Cavet, J. S.; Tabernero, L. *J. Antimicrob. Chemother.* **2009**, *63*, 928–936.
(31) Grundner, C.; Perrin, D.; van Huijsduijnen, R. H.; Swinnen, D.; Gonzalez, J.; Gee, C. L.; Wells, T. N.; Alber, T. *Structure* **2007**, *15*, 499–509.
(32) Grundner, C.; Ng, H. L.; Alber, T. *Structure* **2005**, *13*, 1625–1634.
(33) Nam, H. J.; Poy, F.; Krueger, N. X.; Saito, H.; Frederick, C. A. *Cell* **1999**, *97*, 449–457.

connected; a large excursion of helix α8 is possible with little change in the position of α7. In addition, the PtpB/OMTS structure reveals the folding of a new helix (α3a) in the β3-α4 loop on the edge of the active site (Figures 1b,e).[31] PtpB is active in solution but not in its crystalline form.[32] Considering that both available crystal structures have the lid closed and that significant packing forces are expected in a protein crystal, it can be inferred that the lid must open for substrate binding and catalysis to occur. These observations strongly suggest that the α7−α8 lid and the β3−α4 loop comprise mobile elements that undergo large excursions during substrate turnover.[31]

Since the closed lid blocked substrate binding and inhibited PtpB activity, Grundner et al. determined whether the lid also offers protection from oxidative inactivation.[32] Of all PTPs tested at that time, PtpB was the most resistant to inactivation by the physiological oxidant, H_2O_2. A recent report revealed that the PTP proteins SHP-1 and SHP-2 show a similar qualitative resistance to oxidative inactivation.[34] This resistance was attributed in part to an N-terminal SH2 domain (N-SH2) that folds over the catalytic site, blocking access of substrates and ROS.[34] Binding of a pTyr peptide to the N-SH2 domain promoted an unusual allosteric transition that exposed the active site.[34] These observations further support the hypothesis that the PtpB lid may serve as a dynamic filter that protects the catalytic cysteine from modification during the oxidative burst in macrophages[35] or as a result of ROS produced by cellular signaling events.[36]

PtpB represents an interesting challenge in that the protein remains poorly characterized other than its crystal structure. In this work, in addition to generally investigating the molecular mechanics underlying its large-amplitude conformational transitions, we also illustrate how, as guided by the strategic questions mentioned earlier, new insights regarding PtpB conformational dynamics and biochemistry can be obtained by integrating known structural and biological information with single-molecule protein dynamics. Using single-molecule fluorescence measurements, oxidation assays, limited proteolysis, and kinetic modeling, we test the hypothesis that the *Mtb* PtpB lid provides a dynamic filter that excludes oxidants and affords substrate access. Using recently developed high-resolution time-dependent single-molecule spectroscopy,[18,37,38] we found that the PtpB lid spontaneously transits from the previously observed closed conformation to a much more open conformation that has not been captured crystallographically. By altering the time resolution of the analysis of single-molecule FRET measurements, we determined the opening and closing rates of the PtpB lid. The populations of closed and open conformers determined from a two-state model showed that the closed conformer exists ~75% of the time. Assuming the closed form protects the active site from oxidation, the rates of lid opening and closing quantitatively account for the measured rates of inactivation by ROS. Overall, our results revealed that PtpB switches rapidly between closed and open conformers in which the closed population limits access of ROS and substrates to the active site and the open population is required for enzymatic activity.

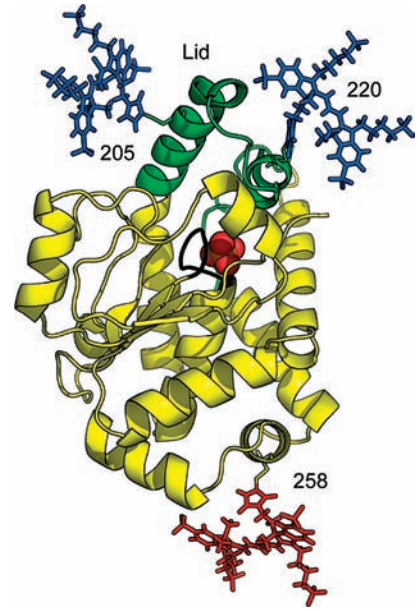

Figure 2. Ribbon diagram of the constructs used for single-molecule FRET experiments. Labeling positions Glu205, Val220, and Arg258 have been mutated to cysteine, and sample dyes have been modeled onto the structure by hand (red and green line structures). The active-site loop has been colored black, while the lid has been colored green. The inorganic phosphate bound to the protein active site is represented with a space-filling model.

These studies establish dynamic tuning of protein conformation as an important protective mechanism for the PtpB enzyme.

To further examine the role of lid dynamics, oxidative inactivation of PtpA and PtpB was systematically examined under varying viscosities. PtpB (but not PtpA) showed viscosity-dependent active-site oxidation in glycerol solutions but not in solutions containing PEG8000, a viscosogen believed to be too bulky to interfere with microscopic conformational dynamics.[39] Single-molecule FRET measurements indicated that this effect was due to a shift toward open conformers caused primarily by an increase in the opening rate compared with PtpB in the absence of glycerol. Additionally, single-molecule experiments were conducted to independently measure the opening and closing rates of the two PtpB lid helices, α7 and α8. Although one may expect that these adjacent helices move as a single structural element, it was found that the helices are capable of moving asynchronously, suggesting that lid opening and closing is structurally more complicated than a concerted two-state process involving both helices. Further investigations applying limited proteolysis under different viscosities suggest that the local folding and unfolding of the α3a helix may influence the conformational dynamics of lid helix α8.

Experimental Section

Unless specified, all experiments were carried at room temperature (21.7 ± 0.3 °C).

PTP Expression and Purification. PtpB was expressed in *E. coli* and purified as described.[32] Point mutations were generated by PCR reactions using mutagenic primers. With the PtpB/PO_4 structure as a guide, cysteine residues were introduced at solvent-exposed sites in the lid to create two double mutants for FRET experiments, Glu205Cys-Arg258Cys (abbreviated Glu205Cys), to probe helix α7 and Val220Cys-Arg258Cys (abbreviated Val220Cys) to probe the α8 helix (Figure 2). In the PtpB/PO_4 crystal structure,

(34) Weibrecht, I.; Bohmer, S. A.; Dagnell, M.; Kappert, K.; Ostman, A.; Bohmer, F. D. *Free Radic. Biol. Med.* **2007**, *43*, 100–110.
(35) Rao, G. N. *Oncogene* **1996**, *13*, 713–719.
(36) Monteiro, H. P.; Arai, R. J.; Travassos, L. R. *Antioxid. Redox Signal.* **2008**, *10*, 843–889.
(37) Watkins, L. P.; Yang, H. *Biophys. J.* **2004**, *86*, 4015–4029.
(38) Watkins, L. P.; Chang, H. Y.; Yang, H. *J. Phys. Chem. A* **2006**, *110*, 5191–5203.
(39) Blacklow, S. C.; Raines, R. T.; Lim, W. A.; Zamore, P. D.; Knowles, J. R. *Biochemistry* **1988**, *27*, 1158–1167.

the C_β atoms of Glu205 and Arg258 are separated by ~43 Å. Arg258 was chosen as a reference labeling position since it is predicted by the available crystal structures to be on the surface of the core PTP fold at a suitable distance from the lid to detect lid opening using FRET (Figure 2). Additional criteria used for labeling position choice are that all residues have their side chains oriented into solution and neither of the charged residues (Glu205 or Arg258) are involved in salt bridges. Although the protein active site contains a single native cysteine, reaction conditions containing excess product were developed to prevent labeling of this residue with maleimide dyes (see below).

PtpA was amplified from genomic DNA of the *Mtb* H37Rv strain (Colorado State University). PCR products were cloned in frame with an N-terminal His_6tag in the pET28b expression vector (Novagen). For protein expression, plasmids were transformed into BL21 (DE3)-CodonPlus cells (Stratagene) and grown in Terrific Broth containing 50 mg/mL of kanamycin and 34 mg/mL of chloramphenicol at 37 °C to an OD_{600} of 0.5. After addition of 100 mM IPTG, the cultures were grown for an additional 20 h at 20 °C. The cells were harvested by centrifugation and resuspended in 20 mM Tris (pH 7.5), 100 mM NaCl, and 10% glycerol. The protein was purified by immobilized metal affinity chromatography (Ni-NTA Agarose, Qiagen) and size-exclusion chromatography (Superdex S75, GE Healthcare). The protein eluted from the size-exclusion column in 20 mM Tris (pH 7.5), 100 mM NaCl and was concentrated to 5 mg/mL.

YopH was cloned, expressed, and purified as described previously.[40]

PtpB Labeling. PtpB proteins were reduced with 1.0 mM tris(2-carboxyethyl)phosphine (TCEP; Sigma Aldrich). Each PtpB cysteine variant was labeled simultaneously with the dyes Alexa Fluor C2 maleimide 555 (FRET donor dye, Invitrogen) and Alexa Fluor C2 maleimide 647 (FRET acceptor, Invitrogen). To prevent labeling of the active-site cysteine, the proteins (150 μM) were labeled in 1 M K_2HPO_4. Reactions were carried out overnight at 4 °C and protected from light. The labeled protein was separated from free dyes using a Superdex 75 gel filtration column (HR-10/30, GE Healthcare) in 20 mM tris(hydroxymethyl)aminomethane (adjusted to pH 7.5 using HCl, abbreviated Tris-HCl) and 100 mM NaCl. To remove PO_4 from the sample, the protein was separated four times on Micro Bio-Spin 6 columns (BioRad) equilibrated in 20 mM Tris−HCl pH 7.5, 100 mM NaCl. Neither ESI-MS on a quadrupole time-of-flight mass spectrometer nor MALDI-MS was able to detect unlabeled or singly labeled proteins; thus, the labeling efficiency was assumed to be 100% for the purposes of enzymatic activity and bulk FRET calculations. This labeling protocol did not affect the specific activity of the enzyme when assayed with p-nitrophenylphosphate (pNPP; Table S1, Supporting Information).

Single-Molecule FRET Experiments. Single-molecule FRET experiments were performed on a confocal microscope as described previously.[18,38] Briefly, dye-labeled, His_6-tagged PtpB molecules were immobilized on a biotin-PEG derivatized quartz coverslip with biotinylated α-His_6 antibodies (Rockland Immunochemicals) bound to streptavidin (Jackson ImmunoResearch)[18] in 20 mM Tris−HCl at pH 7.5 with 100 mM NaCl. A continuous wave diode-pumped solid-state (CW-DPSS) Nd:YAG laser (532 nm, Coherent Compass 315M) was used as a light source, and two avalanche photo diodes (APD, Perkin-Elmer SPCM-AQR13) operating in single-photon counting mode were used for data collection.[38] Raw single-molecule photon arrival data were analyzed following the maximum-information method (MIM) where distance measurements (bins) were made according to the criteria that each had a constant amount of relative error. The relative error bounds in the MIM were a user-adjustable parameter in the analysis algorithm and were evaluated according to principals from information theory.[18,37,38] This procedure resulted in distance measurements containing variable apparent bin sizes.

Distance measurements were used to construct raw single-molecule probability density functions (PDFs) by assuming a Gaussian kernel density estimator.[37] Since each distance measurement had a constant, well-characterized amount of error, maximum entropy deconvolution was used to remove broadening due to photon-counting noise from the PDFs. Deconvoluted PDFs presented were constructed by combining distance-vs-time data from more than 150 individual molecules. To extract kinetic parameters from the single-molecule experiments, data analysis was performed at nine different time resolutions over the range of 2−10 ms. Changes in analysis time resolution were achieved by varying the accuracy of the MIM data analysis over a range of 7−15% relative error. Lower relative error required more photons per time bin and thus had a slower average time resolution.

A two-state motional narrowing model describing the average dye separation distance of the open and closed conformations, the rates of lid opening and closing, and the time-dependent Gaussian width of each PDF was globally fit to the nine time-dependent PDFs. For the Glu205Cys mutant in 25% glycerol, six probability density functions (covering time-resolutions in the range of 3−5 ms) were used for the global fitting because this protein displayed opening and closing rates near our highest time resolution and inclusion of the nearly identical slower time-resolution PDFs biased the global fitting.

To rule out the possibility that the measured conformational dynamics are due to dye−protein interactions on the experimental time scale, single-molecule polarization−modulation experiments were performed following procedures described previously.[18] Here, the polarization of a linearly polarized laser was modulated by 90° at a frequency of 340 Hz using a Pockel's cell (Model 350−50, Conoptics). The lack of correlation in the intensity autocorrelation function indicated that there were no significant interactions between the fluorophores and the protein on our experimental time scale (Figure S9, Supporting Information). Error bounds for the autocorrelation functions were calculated using the analytical expression reported previously.[41]

Steady-State FRET Spectroscopy. Steady-state FRET experiments were carried out on a fluorescence plate reader (Molecular Devices, M5). Data were analyzed by the method of enhancement of acceptor emission.[18,42] The Förster radius (R_0) for the dye pair Alexa Fluor 555 and Alexa Fluor 647 (Molecular Probes) was calculated according to the spectral overlap between the donor emission and acceptor absorbance

$$R_0^6 = 0.772\kappa^2 n^{-4}\Phi_D \int_0^\infty \varepsilon_A(\lambda)F_D(\lambda)\lambda^4 d\lambda$$

where κ^2 is the dye orientation factor (assumed to be 2/3), n is the refractive index, Φ_D is the donor quantum yield, $\varepsilon_A(\lambda)$ is the wavelength-dependent acceptor extinction coefficient, and $F_D(\lambda)$ is the normalized donor emission spectra.[43] Calculations were carried out in solutions with 0, 5, 10, 15, and 25% glycerol and PEG-3000. Extinction coefficient for both dyes were calculated using the manufacturer's published values in methanol as a reference, 158000 and 265000 M^{-1} cm^{-1} for Alexa 555 and Alexa 647, respectively.[44] Donor quantum yield was calculated by comparison with Rhodamine 6G in water as a standard, $\Phi_{R6G} = 0.90$.[45] Refractive index was measured on an Abbe refractometer (Model 120597, Carl Zeiss). The calculated R_0 for the Alexa Fluor 555/647 dye pair was found to be 51 ± 0.9 Å in buffer, 54.0 ± 0.9 Å in buffer containing 25% glycerol, and 52.6 ± 0.9 Å in buffer

(40) Seeliger, M. A.; Young, M.; Henderson, M. N.; Pellicena, P.; King, D. S.; Falick, A. M.; Kuriyan, J. *Protein Sci.* **2005**, *14*, 3135–3139.
(41) Hanson, J. A.; Yang, H. *J. Chem. Phys.* **2008**, *128*, 214101.
(42) Clegg, R. M. *Methods Enzymol.* **1992**, *211*, 353–388.
(43) Lakowicz, J. R. *Principles of Fluorescence Spectroscopy*, 2nd ed.; Springer: New York, 1999; pp 298−301.
(44) Haugland, R. P.; Spence, M. T. Z.; Johnson, I. D. *The Handbook: A Guide to Fluorescent Probes and Labeling Technologies*, 10th ed. [online]; Invitrogen: Carlsbad, CA, 2005.
(45) Magde, D.; Wong, R.; Seybold, P. G. *Photochem. Photobiol.* **2002**, *75*, 327–334.

Scheme 1. Kinetic Model for PtpB Inactivation by H_2O_2

$$PtpB_{closed} \underset{k_{close}}{\overset{k_{open}}{\rightleftharpoons}} PtpB_{open} \xrightarrow{k_{inact,PtpA}[H_2O_2]} PtpB_{inactive}$$

containing 25% PEG-3000. See Figure S10 and Table S3 (Supporting Information) for spectral data and R_0 values.

Enzyme Kinetics. The final concentration of the labeled PtpB proteins was determined by A_{280} readings using the extinction coefficient to determine concentration. Phosphatase assays were performed in 96-well plates using pNPP (Sigma Aldrich) at concentrations ranging from 0.1−125 mM in 20 mM Tris−HCl pH 7.5, 100 mM NaCl, 10 mM DTT at 100 nM enzyme concentration. Reactions were initiated by adding pNPP, and A_{405} was measured in a continuous assay using a SPECTRAmax 190 spectrophotometer (Molecular Devices). The initial rates were calculated from the slope of the change in absorbance versus time. The kinetic parameters V_{max} and K_M were determined using nonlinear regression fit of the initial velocity versus substrate concentration curve using Sigma Plot v 9.0 (Systat Software, Inc.). The k_{cat} was determined by dividing the *V*max by the molar enzyme concentration and standard errors were calculated.

For oxidation inactivation measurements, PtpB proteins were fully reduced with 10 mM DTT for 30 min at room temperature. To remove DTT, the proteins were buffer exchanged through four consecutive Micro Bio-Spin 6 columns. The viscosogens glycerol and PEG8000 were added to final concentrations of 0−25%. PtpB variants were inactivated with 62.5−1000 μM H_2O_2 for 0−45 min. Aliquots were removed at time points ranging from 0 to 45 min and added to a solution of 125 mM pNPP in 20 mM Tris at pH 7.5 with 100 mM NaCl for 5 min. The reactions were terminated with the addition of 2 M NaOH to a final concentration of 0.4 M NaOH. The A_{440} was read using the Molecular Devices spectrophotometer. The resulting curves of normalized PtpB activity versus time were fit using SigmaPlot 9.0 (Systat Software, Inc.) to a single exponential whose decay constant was assumed to be $k_{inact,app}[H_2O_2]$. The slope of $k_{inact,app}[H_2O_2]$ versus $[H_2O_2]$ gave k_{inact}.

Kinetic Modeling of Inactivation. To model PtpB inactivation by H_2O_2, we assumed that the protein exists in open and closed conformations and that only the open conformation can be inactivated by H_2O_2 (Scheme 1). For this model, the opening and closing rates were taken from single-molecule experiments, and the measured inactivation rate of *Mtb* PtpA was used to estimate the inactivation rate of the open conformer. Differential equations corresponding to the kinetic scheme were solved numerically with the ordinary differential equation (ODE) solver in MATLAB 7.3. The simulations used 1.6 μM PtpB and were carried out 10 times for 8000 s over a H_2O_2 concentration range of 62.5−1000 μM. The value of $k_{inact,app}$ was determined from the slope of the dependence of the inactivation rate on peroxide concentration. Error bars were estimated by Monte Carlo simulations (bootstrap) according to the errors in the measured values of k_{open}, k_{close}, and $k_{inact,PtpA}$.

Limited Proteolysis. PtpB was incubated with 1000:1 (w/w) trypsin in 20 mM Tris−HCl, 100 mM NaCl (pH 7.5) with and without 25% glycerol at room temperature. It has been shown that trypsin reactivity in 3 M glycerol (~26% w/w) is comparable to that in aqueous buffer.[46] Samples were taken at various time points, and proteolysis was stopped by the addition of SDS-PAGE loading buffer to a final SDS concentration of 1%. The samples were run on a 4−12% NuPAGE gel and stained with Coomassie blue.

Results and Discussion

X-ray crystallographic studies revealed novel features, including a closed-lid structure that blocks the active site, that distinguish *Mtb* PtpB from conventional PTPs.[32] PtpB shows potent phosphatase activity in solution, but catalytic activity is inhibited in crystals in which access to the active site is blocked. These observations implied that the PtpB lid must move in solution in order to expose the active site, allowing substrate binding and catalysis.

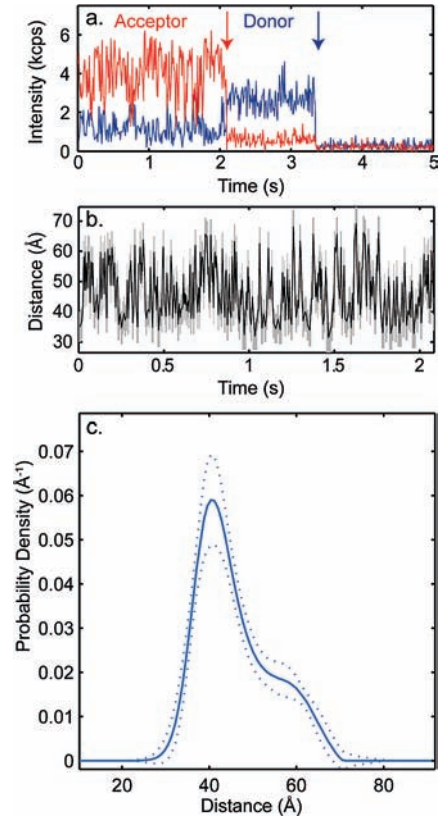

Figure 3. Single-molecule FRET data reveal interconverting open and closed forms of PtpB in solution. (a) Time-dependent fluorescence emission intensity for a single PtpB molecule labeled at Glu205Cys in helix α7 and displayed at a 10 ms bin size. Acceptor emission is denoted by a red line and donor emission by a blue line. Arrows indicate the time at which each dye bleached. (b) Visualization of the lid dynamically switching between the closed and open conformations. Distance trajectory created from the emission intensity using the maximum-likelihood method,[37] where the gray boxes represent the uncertainty of the time of each measurement along the *x*-axis and uncertainty in the position of each measurement along the *y*-axis. (c) Probability density functions (3 ms time resolution) for Glu205Cys (α7) created from more than 150 individual single-molecule fluorescence trajectories using the maximum entropy deconvolution method.[38] Dotted lines represent the error bounds for each PDF, showing that the bimodal distributions are indeed statistically significant.

Direct Observation of PtpB Lid Dynamics in Solution. The most unexpected feature of the PtpB/PO_4 structure was the two-helix lid that blocks the active site (Figure 1). When compared to other sequences, the lid (residues 197−235, green region in Figure 2) represents an insertion unique to PTPs from mycobacteria. The lid begins in helix α7, a long α helix that includes two full turns of a 3_{10} helix (residues 190−196). Helix α7 ends at residue Asp212 and is connected by a five-residue linker to α8 (residues 218−225), which is followed by a 10-residue loop.

We used single-molecule FRET to determine whether the PtpB lid opens and closes spontaneously in solution. Figure 3a displays a representative single-molecule intensity-versus-time trajectory of the Glu205Cys-Arg258Cys double mutant protein (abbreviated Glu205Cys), which probes the conformation of helix α7 at 3.6 ms time resolution. Maximum-information

(46) Kumar, R.; Serrette, J. M.; Thompson, E. B. *Arch. Biochem. Biophys.* **2005**, *436*, 78–82.

Table 1. Numerical Results of Fitting to the Two-State Motional Narrowing Model

	Glu205Cys	Val220Cys	Glu205Cys 25% glycerol
k_{open}	$140 \pm 40\ s^{-1}$	$60 \pm 30\ s^{-1}$	$320 \pm 50\ s^{-1}$
k_{close}	$380 \pm 100\ s^{-1}$	$180 \pm 60\ s^{-1}$	$260 \pm 40\ s^{-1}$
R_{open}	62 ± 2 Å	57.7 ± 0.8 Å	64 ± 2 Å
R_{close}	39.8 ± 0.6 Å	37.6 ± 0.4 Å	41 ± 1 Å
F_{open}	0.27 ± 0.04	0.26 ± 0.03	0.55 ± 0.04
F_{close} [a]	0.73 ± 0.04	0.74 ± 0.03	0.45 ± 0.04

[a] The fraction closed (F_{close}) can be estimated by $F_{close} = k_{close}/k_{tot}$, where $k_{tot} = k_{open} + k_{close}$.

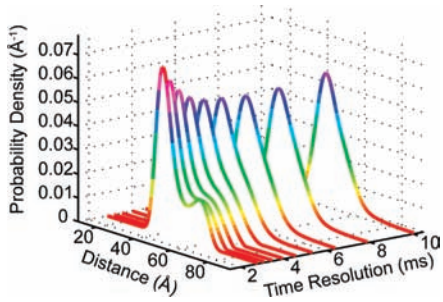

Figure 4. Time-dependent probability density functions for the Glu205Cys PtpB mutant used to calculate the rates of lid opening and closing. These panels were constructed by systematically varying the error tolerance while reanalyzing the same data set;[18] for each error tolerance level, the time resolution is inversely proportional to the square-root of the error tolerance.[37] The conversion of the two modes in the probability density functions at the highest time resolutions to one mode (that is the average of the two high-resolution peaks) at lower time resolutions was used to extract the lid opening and closing rates.[18,47,48] These results imply that the two populations are dynamically interconverting on a time scale similar to the experimental time resolution.

analysis[37] of the data produced the sample distance vs time trajectory (Figure 3b), which reveals that the lid fluctuates over widely different distances. The maximum-information analysis extracts donor−acceptor separations in terms of normalized distances, $x = R/R_0$, where R is the apparent distance and R_0 is the Förster radius. Hereafter, R_0 is assumed to be 51 Å in buffer and 54 Å in 25% glycerol, as estimated from the spectral overlap. The shortest apparent distances are consistent with that of the closed-state observed in the PtpB/PO_4 crystal structure, while the more extended distances demonstrate that open conformers are also populated, albeit transiently.

To determine the populations of conformations accessible to the lid, a probability density function (PDF, Figure 3c) was created using the model-free, maximum-entropy deconvolution method[38] to analyze data recorded from more than 150 individual molecules. Rather than populating a single-mode, continuous distribution, PtpB displayed a bimodal distribution of distances. The single-molecule experiments revealed an open state of PtpB that has not been observed in previous crystallographic studies. In the open state, the probe on the lid helices moves 10−20 Å away from Arg258 compared to the closed form (Table 1).

To evaluate the rates of lid opening and closing, we constructed the deconvoluted PDFs at time resolutions between 2−10 ms.[18] The two conformational modes resolved at the highest time resolutions coalesced into a single distribution that represents the average position of the two peaks (Figure 4). These results indicate that the lid opens and closes on time scales similar to our experimental time resolution, a process analogous to motional narrowing in NMR and optical spectroscopy. By globally fitting the time-dependent conformational PDFs to a two-state motional narrowing model,[18,47,48] we determined the rate constants for opening and closing (k_{open} and k_{close}) as well as the distance between the fluorophores in the open and closed conformations (R_{open} and R_{close}). The results are summarized in Table 1 (see also Table S2 and Figures S1 and S2, Supporting Information). Based on these rate constants, the ratio of closed/open conformers for the Glu205Cys mutant labeled on helix α7 was $(0.73 \pm 0.04)/(0.27 \pm 0.04)$. These results demonstrated the existence of an open conformation of PtpB lid.

Table 2. Rates of Oxidative Inactivation of PtpB Compared with the Lidless PTPs VHR, LAR, and PTP1

PTP	k_{inact} ($M^{-1}s^{-1}$)
VHR[a,b]	17.9 ± 1.3
LAR[a,b]	14 ± 3.1
PTP1[a,b]	9.1 ± 0.1
Yersinia pestis YopH[a]	14.78 ± 0.43
Mtb PtpA[a]	10.17 ± 1
Mtb PtpB	2.1 ± 0.3

[a] This is a lidless phosphatase variant. [b] Data from ref 49.

Correlation of Lid Dynamics with Oxidative Inactivation. To explore the relationship between lid motions and the high resistance of PtpB to oxidative inactivation, we measured the rate at which peroxide targets the Cys160 nucleophile. As controls, we created several deleted lid PtpB constructs with varied connection sites and linker lengths, but these proteins had greatly reduced k_{cat} values (at least 35-fold lower), expressed poorly, and could not be obtained in large quantities. Because these properties precluded a direct comparison, we measured the inactivation rates of wild-type PTP proteins from *Mtb* (PtpA) and *Yersinia pestis* (YopH) that lack a protective lid. PTP proteins were treated with a range of H_2O_2 concentrations (62.5−1000 μM) for 0−45 min, and inactivation was followed using an enzymatic assay. The measured second-order rate constants for inactivation, k_{inact}, indicated that PtpB was oxidized at least 5-fold more slowly than the lidless, structurally homologous phosphatases LAR, VHR, PTP1,[49] YopH, and PtpA (Table 2).

To further understand the mechanism of oxidation protection of PtpB, we developed a kinetic model in which only the open conformer is inactivated by H_2O_2 (Scheme 1). We used the lid opening and closing rates measured by single-molecule FRET as well as the inactivation rate of *Mtb* PtpA to predict the apparent H_2O_2 inactivation rate of PtpB. While we recognize that there are significant differences in substrate specificity and structure between PtpA and PtpB, we emphasize that the purpose here is to obtain a qualitative trend comparing the oxidative inactivation of PtpB to a representative PTP without a lid. The assumption that the open conformer of PtpB is inactivated at approximately the rate of PtpA is reasonable, since several PTPs lacking a lid showed similar rates of inactivation by peroxides (Table 2). Assuming that the closed conformer protects PtpB from ROS inactivation, this model predicts an apparent inactivation rate constant of $2.7 \pm 0.8\ M^{-1}\ s^{-1}$ for Glu205Cys PtpB, in close agreement with the measured rate of $2.1 \pm 0.3\ M^{-1}\ s^{-1}$ for the wild-type enzyme. Because the effective inactivation rate at high μM H_2O_2 concentrations is much slower than the lid opening and closing rates, protection of the PtpB active site can be understood as a thermodynamic mechanism in which the degree of protection is determined by the relative populations

(47) Geva, E.; Skinner, J. L. *Chem. Phys. Lett.* **1998**, *288*, 225–229.
(48) Gopich, I. V.; Szabo, A. *J. Phys. Chem. B* **2003**, *107*, 5058–5063.
(49) Denu, J. M.; Tanner, K. G. *Biochemistry* **1998**, *37*, 5633–5642.

of open and closed conformers rather than by the opening and closing rates directly.

Effects of Solvent Viscosity on Oxidation and Lid Dynamics. To further test the hypothesis that the PtpB lid protects the active site from oxidation and to gain insights about PtpB activity in a viscous cellular environment, we carried out H_2O_2 inactivation assays while systematically increasing the solvent viscosity. Viscosogens have been used previously to probe rate-determining steps of reactions involving large-scale conformational changes that affect processes such as catalysis and protein folding.[50,51] If the lid dynamics limit PtpB inactivation, a solute like glycerol that increases microscopic and macroscopic viscosity would be expected to increase the rate of inactivation by slowing lid closing. In contrast, the larger, polymeric viscogen, PEG8000, will be excluded from the protein and should not significantly affect lid dynamics, resulting in little or no change in the peroxide inactivation rate. A limitation of this approach is that these solutes can potentially alter inactivation by modulating the relative stability of the closed and open forms.[51]

For wild-type PtpB, the rate of oxidative inactivation increases in the presence of glycerol and not PEG8000 (Figure 5a). The increase in inactivation rate scaled with the concentration of glycerol, where a 1.8-fold increase in k_{inact} was observed in 10% glycerol and 4-fold increase was seen in 25% glycerol (Figure 5a). The rates of inactivation of PtpA were not affected by either glycerol or PEG8000 (Figure 5a), pointing to the possibility that the extent of oxidation of PtpB is associated with a conformational change in the lid. Measurements of the bulk FRET efficiencies of the Glu205Cys PtpB variants indicated that glycerol shifts the population to more open forms than seen in the presence of PEG8000 (Figure 5b). These results are consistent with the idea that the open form mediates susceptibility of the protein to peroxide inactivation.

To establish the mechanism by which glycerol increases the rate of PtpB oxidative inactivation, we performed single-molecule FRET experiments with the Glu205Cys protein in the presence of 25% glycerol (Figure 5c). As observed in the absence of glycerol, the lid displayed a bimodal distribution of distances with $R_{close} = 41 \pm 1$ Å and $R_{open} = 64 \pm 2$ Å, similar to the apparent distances obtained in the absence of glycerol (see Table 1 as well as Table S2 and Figures S6−S8, Supporting Information). The presence of 25% glycerol caused a striking shift in the population of conformers to the open form (Figure 5c), with the ratio of closed/open conformers equal to $0.45 \pm 0.03/0.55 \pm 0.03$ (compared to 0.73/0.27 in the absence of glycerol). Unexpectedly, this decrease in the relative population of the closed form was dominated by an increase in the opening rate in the presence of 25% glycerol ($k_{open} = 320 \pm 50$ s^{-1} and $k_{close} = 260 \pm 40$ s^{-1}), rather than slower closing of the lid. The rates of the lid motions in the presence of 25% glycerol nonetheless correctly predicted the trend in the oxidative inactivation rates. Using the kinetic model in which only the open conformations are sensitive to peroxide (Scheme 1) predicted $k_{inact,app} = 5.7 \pm 0.6$ M^{-1} s^{-1} in 25% glycerol, compared to the measured inactivation rate constant of 7.6 ± 0.1 M^{-1} s^{-1}. These results reinforce the notion that PtpB lid protects the active site from oxidative inactivation through a dynamic gating mechanism.

A protective role for the lid also was supported by the faster oxidation of PtpB in 25% glycerol but not 25% PEG 8000.

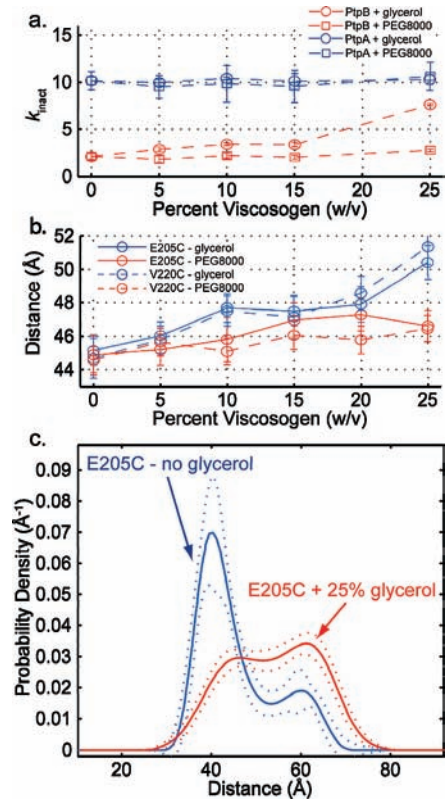

Figure 5. Glycerol, but not PEG 8000, alters the oxidative inactivation rate and dynamics of the PtpB lid. (a) Measured rate constants (k_{inact}) for peroxide inactivation of PtpA and PtpB in the presence of viscosogens glycerol and PEG8000. Glycerol changes the inactivation rate of PtpB, while the bulkier PEG8000 has little effect, presumably because PEG 8000 is excluded from the protein volume. *Mtb* PtpA inactivation is unaffected by both viscosogens. (b) Distance measured from bulk FRET measurements of labeled Glu205Cys (E205C, lid helix α7) and Val220Cys (V220C, α8) PtpB as a function of glycerol and PEG8000 concentration. The distance between the fluorophores increases more with added glycerol than with PEG8000, consistent with an increasing population of the open conformer in the presence of glycerol. (c) Distance PDFs obtained from single-molecule FRET experiments performed on labeled Glu205Cys (E205C) PtpB in the presence (red lines) and absence (blue lines) of 25% glycerol. R_0 in 25% glycerol = 54.0 Å. Glycerol increases the relative populations of the open conformers, such that the open and closed forms are nearly equally populated. Dotted lines represent the error bounds for each PDF. These results indicate that the increased oxidative inactivation rate in the presence of glycerol is associated with changes in PtpB lid dynamics.

These results are in accord with the classic view that, owing to its larger size, PEG 8000 may be excluded from the volume around the protein and have little effect on the local viscosity. Although the macroscopic viscosity is similar in these two solutions, only glycerol changes the microscopic viscosity. As expected from the thermodynamic mechanism, the increased rate of PtpB oxidation in 25% glycerol correlated with an increase in the population of the open form detected by single-molecule FRET spectroscopy (Figure 5c).

The affects of glycerol on large-scale conformational transitions have been interpreted classically in terms of reduced rates of conformational changes that may manifest themselves kinetically in the cases where they play a role in an enzymes mechanism. Knowles and co-workers, for example, proposed that glycerol (but not larger viscosogens) reduced the rate of the reaction catalyzed by triose phosphate isomerase by slowing the closure of the 10-residue loop that covers the active site during turnover.[39,50] The higher microscopic viscosity in the

(50) Sampson, N. S.; Knowles, J. R. *Biochemistry* **1992**, *31*, 8488–8494.
(51) Chrunyk, B. A.; Matthews, C. R. *Biochemistry* **1990**, *29*, 2149–2154.

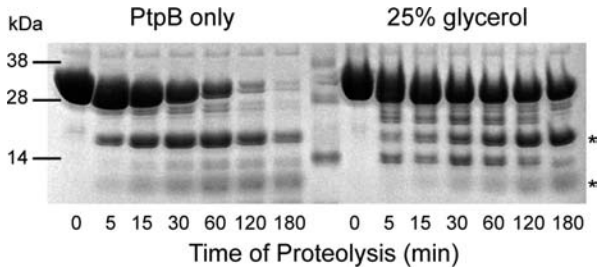

Figure 6. Glycerol protects the PtpB β3-α4 loop from proteolysis. SDS-PAGE gels show the course of partial proteolysis with trypsin in the absence (left) and presence of 25% glycerol (right). The generation of the 11 and 19 kDa products (asterisks) due to cleavage in the β3-α4 loop[31] is inhibited by the presence of 25% glycerol. These results are consistent with the model that the β3-α4 loop is protected by forming helix α3a in the open form.

presence of glycerol was assumed to slow the loop closure by increasing the "friction" on the protein chain.

We tested this paradigm directly using single-molecule FRET to measure the lid dynamics of Glu205Cys in 25% glycerol. Contrary to the classic view, glycerol failed to slow either lid opening or closing. Instead, glycerol shifted the PtpB equilibrium toward the open state by increasing the lid opening rate 2.3-fold with no significant affect on the closing rate (Table 1). While our results do not distinguish the extent to which glycerol alters the opening-closing transition state, the relative stabilities of the open and closed states likely contribute to the changes in lid dynamics.

The population shift toward open conformers observed in the presence of glycerol is consistent with the results of limited-proteolysis experiments. Trypsin was shown previously to rapidly cleave PtpB in the β3-α4 loop, which is disordered in the closed PtpB/PO_4 complex structure.[31] Binding of the inhibitor OMTS allowed the disordered loop to fold into the α3a helix observed in the PtpB/inhibitor complex and offered protection against cleavage by trypsin.[32] A similar protection is observed in the presence of 25% glycerol (Figure 6) raising the possibility that helix α3a is more folded. This observed protection and apparent folding of the β3-α4 loop would be expected to couple to an open conformation of helix α8 in order to avoid a steric clash with the folded structure of α3a.[32] These results suggested that local folding and unfolding of helix α3a (close to helix α8) may be coupled to the opening and closing of helix α8.

Mechanics of Lid Movements. Lid opening involves structural changes comprising a large tertiary rearrangement of both helices α7 and α8. Intuitively, one might expect the lid-opening mechanics to involve a concerted movement by both the α7 and α8 helices. To test this hypothesis, we carried out single-molecule FRET experiments probing the movements of the α8 helix using the Val220Cys-Arg258Cys double mutant (Figure 2) and compared the results to those obtained using a probe in α7 helix (Glu205Cys). Figure 7 shows a single-molecule probability density function (PDF) for Val220Cys constructed from more than 200 individual trajectories with a mean time resolution of 3.5 ms. The measured PDF for α8 is also bimodal and displays shorter distances than the α7 helix, in good agreement with the closed distance predicted from the PtpB/PO_4 crystal structure. The populations of open and closed conformers for the two helices appear similar, consistent with a concerted motion. Further investigation of the opening and closing rates for α8 by fitting the time-dependent PDFs to a two-state motional narrowing model,[18] however, reveals the

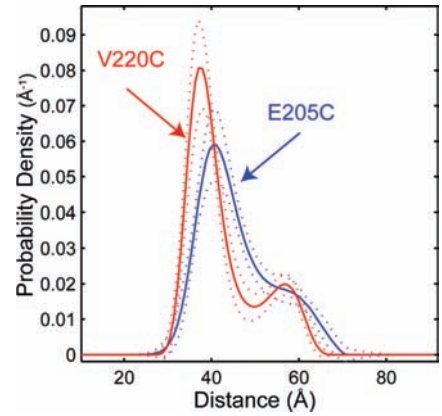

Figure 7. Distance probability density functions comparing the two lid helices, α7 (Glu205Cys, blue E205C) and α8 (Val220Cys, red V220C). The sharper distribution of Val220Cys reflects ~2-fold higher opening and closing rates for helix α8 compared to helix α7.

opening and closing rates of helix α8 to be approximately half of those measured for α7 (Table 1 and Table S2 and Figures S3−S5, Supporting Information). This finding is interesting since it suggests that that helices α7 and α8 move asynchronously. Both lid helices showed similar (~3:1) equilibrium distributions of closed to open conformers; therefore, the differences in the in the α7- and α8-helix kinetics are not likely to result from an equilibrium shift. Due to the large separation of time scales between inactivation at physiological peroxide concentrations and the rates of lid dynamics, our peroxide inactivation model (Scheme 1) predicts nearly identical inactivation rates whether the single-molecule opening and closing rates for Glu205Cys (helix α7) or Val220Cys (helix α8) are used because both probes revealed similar ratios of open and closed conformers.

Although our experiments did not directly probe correlations between the two helices, the differences in kinetics suggest these conformational transitions may involve more complicated local interactions than a simple concerted lid motion. A closer examination of the crystal structures of PtpB/PO_4 and PtpB/OMTS (Figure 1) reveals that asynchronous movement of the two lid helices can be physically accommodated by the protein structure, since a 25 Å displacement of helix α8 is possible while helix α7 remains in the closed conformation. In addition, opening and closing of helix α8 may be correlated with the transient local folding and unfolding of helix α3a. This model is consistent with the results of limited proteolysis experiments in which in an increase in the open population of the lid helix α8 in 25% glycerol (Figure 5b) correlated with an increase in protection of α3a from cleavage by trypsin, potentially due to an increase in the folded helix α3a. A physical coupling between the opening-closing dynamics of helix α8 and the folding-unfolding of helix α3a offers a potential explanation for the reduced rates of conformational dynamics of lid-helix α8 compared to α7.

Summary and Outlook

PtpB is likely to encounter ROS in the host macrophage, where the oxidative burst plays a major role in mycobacterial killing.[52] Additionally, ROS generated in mammalian cells in response to many tyrosine phosphorylation-dependent pathways reversibly inactivate PTP proteins to modulate signaling. The

(52) Miller, R. A.; Britigan, B. E. *Clin. Microbiol. Rev.* **1997**, *10*, 1–18.

oxidation resistance of PtpB mediated by the lid conformational dynamics might represent a novel adaptation by *Mycobacterium* species to oxidative challenges in vivo. Consistent with this idea, PtpB homologues containing a lid occur only in mycobacterial species. The present work presents a direct observation of rich conformational dynamics of the in PtpB lid. The two adjacent lid-helices are capable of independent motion while the measured rates are consistent with a thermodynamic model of active-site protection where ROS only have access to the enzyme active site in the lid-open conformation.

This work also raises interesting possibilities regarding the cellular roles of PtpB. The rapid conformational gating observed in both the opening and closing of the lid serves the twin requirements for recognition of protein substrates and protection from small-molecule oxidants. If the lid and the rim of the catalytic cleft including helix α3a contact the bound protein substrate, recognition would effectively trap an enzyme/substrate complex with the active site unmasked for catalysis. It will be of great interest to identify PtpB's cellular substrates in order to better understand the roles lid conformational dynamics and allostery in substrate recognition and catalysis. The transient blockade of the PtpB active site presented here provides an intriguing insight into the evolution of a fundamentally dynamic molecular mechanism potentially capable of blunting host defenses to *Mtb* infection.

PtpB represents a structurally well-characterized protein whose unique structural elements imply the need for a conformational change. This work illustrates how the combined analysis of structural data, biochemical assays, and high-resolution single-molecule measurements allows tests of specific hypotheses regarding the functional roles of the conformational dynamics. Though a first-principal predictive understanding of large-amplitude conformational transitions will no doubt require a further collaborative integration of theory, experiment, and simulation, the question-guided strategy demonstrated here, and the new insights it helped to uncover, represent an important step toward this goal.

Acknowledgment. We thank C. Grundner for the PtpB gene and purification protocols, Y.-W. Tan and X. Sun for assistance measuring solvent dependent Förster radii, A. Iavarone for MS analysis of labeled proteins, N. Echols for helpful discussions and technical assistance, R. Brem for use of equipment, J.-W. Chu for discussions on protein dynamics, and C. R. Matthews for helpful discussions. This work was supported by the TB Structural Genomics Consortium established by P01 AI68135 (to T.A.) and by R01 GM069937 (to H.Y.) from the National Institutes of Health. The U.S. Department of Energy is acknowledged for use of specialized equipment.

Supporting Information Available: Additional figures and results of data analysis. This material is available free of charge via the Internet at http://pubs.acs.org.

JA909968N